Reprinted from
Vol. 49 No. 3
May/June 2005

The Journal of

Imaging Science and Technology

IS&T
The Society for Imaging Science and Technology
http://www.imaging.org

For information on reprints or reproduction contact
Donna Smith
Managing Editor
The Journal of Imaging Science and Technology
Society for Imaging Science and Technology
7003 Kilworth Lane
Springfield, Virginia 22151 USA
703/642-9090 extension 17
703/642-9094 (fax)
donna.smith@imaging.org
www.imaging.org

Color Visualization System for Near-Infrared Multispectral Images

Meritxell Vilaseca†, Jaume Pujol▲ and Montserrat Arjona
Center for Sensors, Instruments and Systems Development (CD6). Department of Optics and Optometry, Technical University of Catalonia, Terrassa, SPAIN

Francisco Miguel Martínez-Verdú▲
Department of Optics. University of Alicante. Alicante, SPAIN

The aim of this study is to develop a color visualization system for multispectral images in the near-infrared region (NIR, 800–1000 nm). Samples with the same color or appearance in the visible region, which are therefore indistinguishable to the human eye, can have different reflectance or transmittance spectra in other parts of the electromagnetic spectrum, specifically in the NIR. Therefore, these samples can be differentiated by taking into account this extra information. In this work, we use a multispectral system that we have developed recently in order to obtain five images of several samples with varying spectral reflectance, corresponding to different spectral bands. We then define a color space representation which associates the camera responses to the color channels of a calibrated CRT monitor. Therefore, a pseudo-colored image is obtained. Several possible associations are presented, some of them based on methods which attempt to imitate human color vision but in the NIR region, and others for maximizing colorimetric discrimination between the objects, based on principal component analysis (PCA). Finally, the color differences between samples are evaluated using several parameters. The methods which provide the best results in terms of visual discrimination are based on PCA analysis, but the methods related to human color vision keep information of the NIR spectral reflectance of the samples.

Journal of Imaging Science and Technology 49: 246–255 (2005)

Introduction

The near-infrared region of the spectrum (NIR, 800–1000 nm)[1–3] can contain information related to the chemical properties of the objects. Therefore, it is useful in many applications, and can be used as an analytical tool in several fields, such as the textile and chemical industries, environmental science, and military applications. For instance, samples with the same color or appearance in the visible region can differ in spectral terms of reflectance or transmittance in the NIR because of their constituents. Therefore, they may be differentiated by taking into account the extra information provided by this region.

The aim of the process used in this study is to obtain a pseudo-colored image from several NIR, monochrome, multispectral images of a given sample and therefore to visualize the NIR region, which is invisible to the human eye. Because conventional CCD cameras are sensitive to wavelengths up to 1000 nm, we can make use of this standard instrumentation in order to achieve our purpose.

In previous studies,[4–6] we developed a multispectral system composed of a conventional CCD camera and various filters for recovering the spectral reflectances of samples in the NIR region. We performed several simulations and experimental measurements, and analyzed the optimum spectral transmittance of the filters to be used in the setup. We also determined that five channels were enough to perform the reconstructions of the spectral profiles. In this study, we make use of this five-channel configuration, although three bands were enough to obtain a pseudo-colored image, in order to obtain a color visualization system for multispectral images in the near-infrared region. The process that we have used can be divided into the following two main stages:

Definition of the Color Representation Space

Using five monochromatic images of several samples analyzed, which correspond to the different spectral bands of the NIR obtained with the multispectral system, we must define a color representation space in order to obtain a pseudo-colored image.[7,8] Thus, we combine the five multispectral images and generate three new signals (R_{NIR}, G_{NIR} and B_{NIR}) that allow us to obtain a pseudo-colored image. In this article, several possible combinations are proposed, some of them based on methods which attempt to imitate human color vision[9,10] and others that maximize the colorimetric dis-

Original manuscript received July 6, 2004

▲ IS&T Member

†Corresponding Author: M. Vilaseca, Mvilasec@oo.upc.es

Supplemental Material—Figures 7, 8, 10, and 11 can be found in color on the IS&T website (www.imaging.org) for a period of no less than two years from the date of publication.

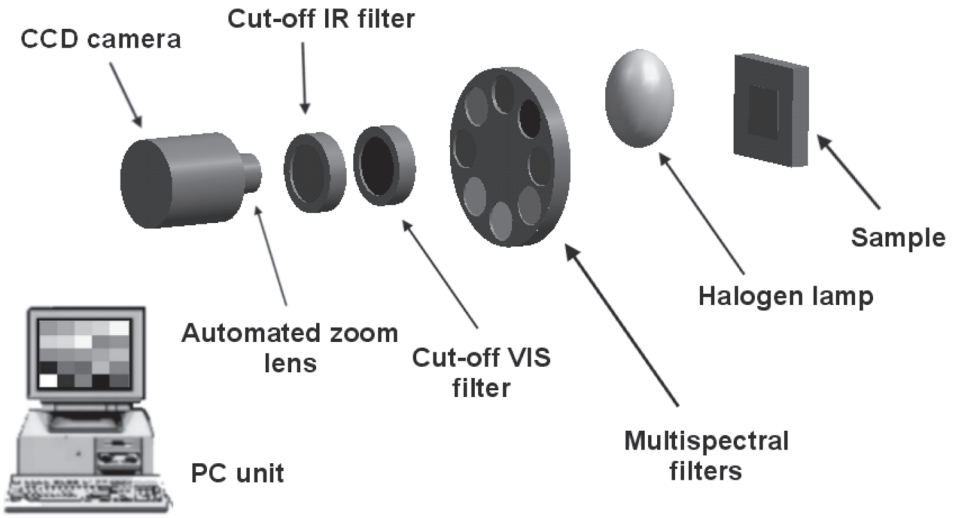

Figure 1. Experimental setup of the NIR multispectral acquisition system.

crimination between objects based on Principal Component Analysis (PCA).[11,12]

Calibration of the Visualization Device

In order to obtain a final pseudo-colored image which is independent of the visualization device used, the R_{NIR}, G_{NIR} and B_{NIR} signals must be adequately transformed. For this purpose, it is necessary to calibrate the display,[13–15] in our case, a conventional CRT monitor, and to define three new signals called $R_{Monitor}$, $G_{Monitor}$ and $B_{Monitor}$, which take into account the characteristics of the primaries and the white of the display. The corresponding digitized signals represent the amount of primaries needed to visualize the final color on the monitor.

Once the two steps described above were carried out, we tested the proposed methodology using five simulated multispectral images corresponding to a set of twenty-five textile samples with different spectral reflectance in the NIR region. Using the simulated images, which allowed better control over the process, we compared the different possible color representations and performed an analysis of the colorimetric differences between the samples using several different parameters, such as pseudo-color differences, contrast levels and CIELAB color differences.

Finally, using the multispectral system developed, we captured several images corresponding to real samples. The pseudo-coloring methods were also applied to these images, and an analysis of the colorimetric results was performed and compared with the previous simulations.

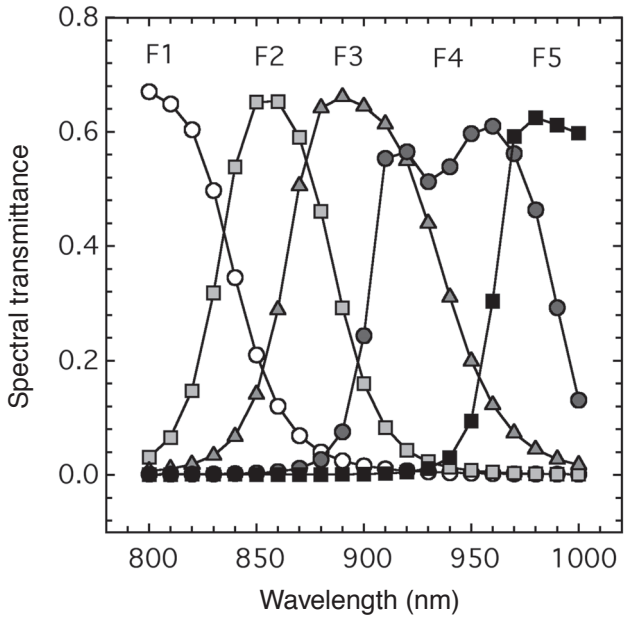

Figure 2. Spectral transmittance of the NIR multispectral filters used in the experimental setup.

Method

Experimental Setup

In this study, we used an NIR multispectral acquisition system (Fig. 1) consisting of a monochrome CCD camera (Photometrics Sensys KAF1400-G2) with a 12 bit depth. An automated zoom lens, which was developed in order to control the exposure of the digital camera, was attached to the camera. The experimental setup involved an illumination system composed of a halogen lamp (Philips 15 V 150 W); five multispectral interference filters (ThermoCorion), which were equispaced in the region studied and which defined the different spectral acquisition bands (Fig. 2); and finally, two more filters, a cutoff IR filter and a cutoff VIS filter (ThermoCorion), which removed the radiation that was not within the NIR range considered.

Definition of the Color Representation Space

Using the experimental configuration described above, we obtained five multispectral images of the samples. Once the five monochrome images were captured, it was necessary to define a color representation to obtain a single pseudo-colored image with a wide range of different colors and therefore a high level of discrimination between samples. Basically, the pseudo-coloring methods used in this study may be classified into the following two groups: methods related to human color vision, and methods maximizing the colorimetric discrimination between samples. The first group attempts to imitate the color vision that the human eye has in the visible range, but for radiation within the NIR re-

gion. The second type includes methods which increase color differences between objects, without taking into account human color vision.

As an initial approximation to the first method, we used linear combinations by directly associating several of the multispectral monochromatic images with the signals R_{NIR}, G_{NIR} and B_{NIR}. The images or spectral bands corresponding to long wavelengths were associated with red, medium wavelengths with green, and short wavelengths with blue. We analyzed several possible combinations; two of these can be seen in Eqs. (1) and (2):

$$\left.\begin{aligned} R_{NIR} &= 0.5\,\mathrm{Im\_F\,4} + 0.5\,\mathrm{Im\_F\,5},\\ G_{NIR} &= \mathrm{Im\_F\,3},\\ B_{NIR} &= 0.5\,\mathrm{Im\_F\,1} + 0.5\,\mathrm{Im\_F\,2}, \end{aligned}\right\} \tag{1}$$

$$\left.\begin{aligned} R_{NIR} &= \mathrm{Im\_F\,4},\\ G_{NIR} &= \mathrm{Im\_F\,3},\\ B_{NIR} &= \mathrm{Im\_F\,2}, \end{aligned}\right\} \tag{2}$$

where $Im\_F_i (i = 1, \ldots, 5)$ are the NIR monochromatic images obtained for the various spectral bands. The first combination (Eq. (1)) uses information from the five multispectral bands of the system while the second combination (Eq. (2)) uses only the three bands that are included in their totality within the NIR region considered (Fig. 2). If we want to perform a pseudo-color visualization, three spectral bands should probably be enough. However, because our experimental system provides five images corresponding to five spectral bands, we use them in order to make full use of all the information available.

A more complex method would be to display a carefully selected combination of the monochromatic images that accounts for the *RGB* responses of the CIE-1931 standard observer,[16] that is, the tristimulus values defined in this color space, but for the NIR region. Translating and compressing the color matching functions of this space into the range analyzed is necessary in order to obtain a behavior in the NIR which is equivalent or similar to that of the visible region. The pseudo-color matching functions in the NIR must be approximated from a combination of the spectral transmittance of the five filters used. This was performed using least squares regression. The mathematical expression of this fitting can be seen in Eq. (3). As shown in Fig. 3, the original, Eqs. (1) and (2), approximated functions differed considerably.

$$\begin{aligned} &R_{NIR} =\\ &0.493\,\mathrm{Im\_F\,1} - 2.075\,\mathrm{Im\_F\,2}\\ &+2.265\,\mathrm{Im\_F\,3} + 0.451\,\mathrm{Im\_F\,4} - 0.133\,\mathrm{Im\_F\,5},\\ &G_{NIR} =\\ &-0.091\,\mathrm{Im\_F\,1} + 0.177\,\mathrm{Im\_F\,2}\\ &+1.296\,\mathrm{Im\_F\,3} - 0.456\,\mathrm{Im\_F\,4} + 0.075\,\mathrm{Im\_F\,5},\\ &B_{NIR} =\\ &0.417\,\mathrm{Im\_F\,1} + 1.036\,\mathrm{Im\_F\,2} -\\ &0.658\,\mathrm{Im\_F\,3} + 0.247\,\mathrm{Im\_F\,4} - 0.042\,\mathrm{Im\_F\,5}. \end{aligned} \tag{3}$$

In addition to the two methods described so far, other typical color appearance models[9,10] used in the visible region can be translated into the NIR region, such as simple *LMS* models (cone excitation space) and more complex models, such as *ATD* (neural or zone) models. *LMS* models simulate the response for each type of photoreceptor and calculate the quantities L, M and S using the tristimulus values of the CIE-1931 standard observer. These values can also be associated with the R_{NIR}, G_{NIR} and B_{NIR} signals (Eq. (4)):

$$\begin{bmatrix} R_{NIR} \\ G_{NIR} \\ B_{NIR} \end{bmatrix} = \begin{bmatrix} L \\ M \\ S \end{bmatrix} = \mathbf{M} \cdot \begin{bmatrix} R \\ G \\ B \end{bmatrix}, \tag{4}$$

where $\mathbf{M}$ is the corresponding transformation matrix which depends on the model considered. Here, the R, G and B signals are the pseudo-tristimulus values of the CIE-1931 standard observer in the *NIR*, obtained using Eq. (3).

More complex color appearance models, such as *ATD*, take into account the opponent colors theory. They usually compute three new signals: A, the achromatic signal, T, the red-green signal, and D, the yellow–blue signal. The A, T, and D signals, which are computed using a different matrix transformation depending on the model applied, can be associated with the R_{NIR}, G_{NIR} and B_{NIR} values as follows:

$$\begin{aligned} R_{NIR} &= A + T \ (\text{if } T > 0) + D \ (\text{if } D > 0),\\ G_{NIR} &= A + T \ (\text{if } T < 0) + D \ (\text{if } D > 0),\\ B_{NIR} &= A + D \ (\text{if } D < 0). \end{aligned} \tag{5}$$

Finally, we studied a further method that we have called the complementary colors model.[7] According to

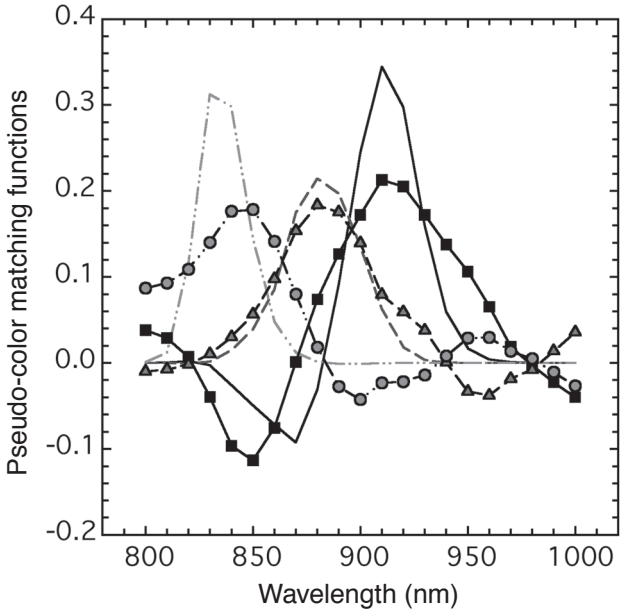

Figure 3. Pseudo-color matching functions corresponding to the CIE-1931 standard observer translated and compressed into the NIR region (lines) and the best approximations obtained from the spectral transmittance of the filters used (lines with symbols).

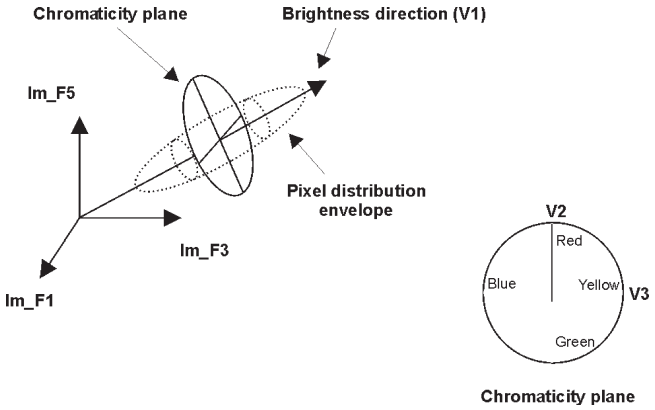

Figure 4. Representation of the color space associated to the modified PCA method, with the corresponding brightness direction and the cromaticity plane.

this model, the monochromatic images corresponding to spectral bands that have longer wavelengths are associated with the R_{NIR} channel, and images corresponding to shorter wavelengths are simultaneously displayed on the G_{NIR} and B_{NIR} channels, thus giving the cyan color. By means of this combination, samples with a high reflectance at long wavelengths appear reddish and samples with high reflectance at short wavelengths are represented as cyan. A sample with a constant reflectance would appear gray. This method is usually used when only two spectral bands are available. Because we have more, we perform a combination of at least three spectral bands in order to use more of the spectral information available in our multispectral system:

$$\begin{aligned} R_{NIR} &= \mathrm{Im\_F\,4}, \\ G_{NIR} &= 0.5\,\mathrm{Im\_F\,2} + 0.5\,\mathrm{Im\_F\,3}, \\ B_{NIR} &= 0.5\,\mathrm{Im\_F\,2} + 0.5\,\mathrm{Im\_F\,3}. \end{aligned} \tag{6}$$

All of the combinations described (methods which attempt to imitate the human color vision) carry spectral information on the samples analyzed. When the reflectance spectra of the samples are fairly constant over the wavelengths of the NIR region, which is common, a high correlation of the different five spectral bands appears. In order to resolve this, we can simply use decorrelation methods that facilitate the colorimetric discrimination between objects. In this case, we first propose using Principal Component Analysis (PCA). Using this method, each pixel can be associated with a vector of five components, which correspond to the gray level of each spectral band. By applying PCA to the set of vectors, i.e., the scene statistics, it is possible to establish a new coordinate system whose axes are in the direction of the eigenvectors, that is, the main directions common to all the pixels of the images. In this way, the mechanism can decorrelate the data. If a high correlation between the different spectral bands exists, many of the samples have a large contribution by the first eigenvector on its components. Thus, we can associate, for instance, the first principal component of the images with a color palette (we have named this method "PCA *V1-Palette*"). The corresponding coefficients are normalized conveniently so they have positive values and can be associated to the digital output levels. Therefore, each pixel will have a specific R_{NIR}, G_{NIR} and B_{NIR} set of values associated with it. On the other hand, we can choose the three principal component directions (eigenvectors related to the three largest eigenvalues) and associate them with the R_{NIR}, G_{NIR} and B_{NIR} signals (PCA *V1-R*, *V2-G*, *V3-B*, for example). With this kind of association, it is possible to assign very different colors to samples with similar reflectance spectra, that is, highly correlated samples. Applying this kind of method, we obtain chromatic discrimination between samples, but the spectral information is lost. In order to overcome this limitation and to keep some spectral information intact, a transformation of this association can be performed. This transformation (modified PCA method), consists of simultaneously associating the first principal component of the scene statistics with the R_{NIR}, G_{NIR} and B_{NIR} signals. Therefore, this component of the pixels accounts for the brightness. The second and third principal components constitute an orthogonal plane to the brightness direction and can be considered a chromaticity plane. For example, considering the conventional rectangular color representation, the second principal vector can be associated with the red–green direction and the third can be associated with the yellow–blue direction. Thus, if the contribution of the pixel analyzed into the direction of the second principal vector is positive, it can be interpreted as red, and, if negative, as green. Equivalently, depending on the sign of its component along the third principal direction, it can be interpreted as yellow or blue. Figure 4 shows the color space associated to this method. In this figure, only three of the five NIR spectral bands are illustrated because of obvious reasons of dimensionality.

Finally, another simple empirical method included in the second group was studied. Using this method, an optimization process maximizing the color difference between samples was performed. Due to the great number of free parameters and the associated resulting high computational cost, we assume that the R_{NIR}, G_{NIR} and B_{NIR} signals must be linear combinations of the five monochrome images and that the coefficients of the combinations must take one of two possible values: 0.1 or 0.9.

Calibration of the Visualization Device

Once the color representation space used to transform the information included in the NIR into visible information is defined, the R_{NIR}, G_{NIR} and B_{NIR} signals obtained must be displayed on a visualization device; in our case, a conventional CRT monitor. Depending on the characteristics of the device used, the samples may appear to be pseudo-colored differently. In order to prevent this, we can previously transform these signals conveniently, taking into account the color calibration of the specific display used. Thus, the final colors represented on the screen will not depend on the monitor used.

The process used to transform the signals is summarized in Fig. 5. First of all, the R_{NIR}, G_{NIR} and B_{NIR} signals were transformed into the tristimulus values X_{D65}, Y_{D65} and Z_{D65}, taking into account the standard space sRGB.[17–19] The CIE sRGB space is defined using an average value for all conventional CRT monitors. The reference white used in this space is illuminant D65. On the basis of this first transformation, we considered that the R_{NIR}, G_{NIR} and B_{NIR} signals corresponded to the signals that would be associated with the channels of the standard monitor of the sRGB space. However, depending on the primaries of the monitor that are actually used, the reference white may not be illuminant D65. For this reason, a chromatic adaptation is needed,[20–22] because it allows a color to be conveniently transformed

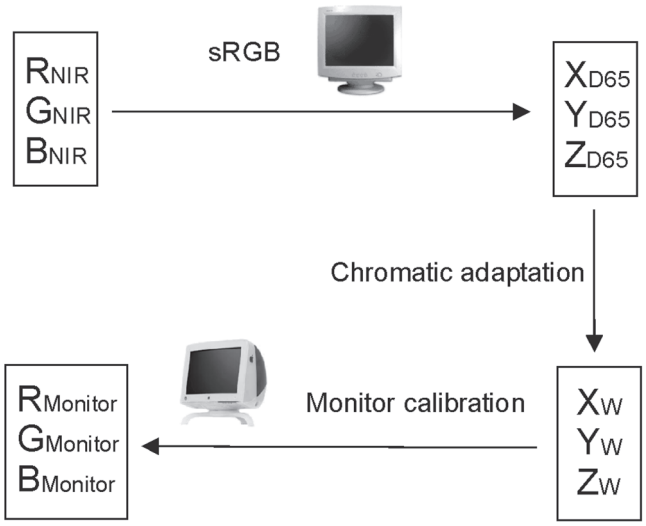

Figure 5. Diagram showing the transformation of the R_{NIR}, G_{NIR} and B_{NIR} signals to $R_{Monitor}$, $G_{Monitor}$ and $B_{Monitor}$, in order to obtain a color visualization that is independent of the monitor used.

TABLE I. Chromaticity Coordinates and Luminance of the Primaries and White of the Monitor Used

	x	y	L_{max} (cd/m^2)
R	0.6246	0.3369	19.50
G	0.3016	0.6015	79.59
B	0.1499	0.0753	11.71
White	0.2884	0.3210	105.4

TABLE II. Parameters of Calibration (GOG) of the Monitor

	gain	offset	γ
R	0.8088	0.1912	2.5170
G	0.9334	0.0666	2.0933
B	0.6938	0.3062	2.8093

so that it gives the same chromatic sensation under illuminant D65 as it would under the new reference white (X_W, Y_W and Z_W). With these new tristimulus values and the color calibration parameters of the monitor used, it is possible to obtain the final digital values that must be associated with the channels of the monitor used ($R_{Monitor}$, $G_{Monitor}$ and $B_{Monitor}$). The method that we used to perform the calibration was the standard GOG (Gamma, Offset, Gain) method defined by the CIE.[13] Using the information of the primaries and the tone reproduction curves of the monitor, which relate the relative luminance of the primaries to the normalized digital output levels for each channel, the GOG model provides the parameters of the color calibration.

In this study, we used a conventional CRT monitor (Hansol) to perform the visualization. The contrast and brightness of the monitor were adjusted in order to obtain a maximum luminance similar to that of the standard monitor (105.4 cd/m^2). The characteristics of the primaries and the white can be seen in Fig. 6 and Table I. The primaries of the monitor used and the standard monitor sRGB cover a similar area of the chromatic diagram, and therefore, for this specific case, the transformation of the signals is small. However, it might be considerable in other cases. The parameters for the color calibration of the monitor are shown in Table II.

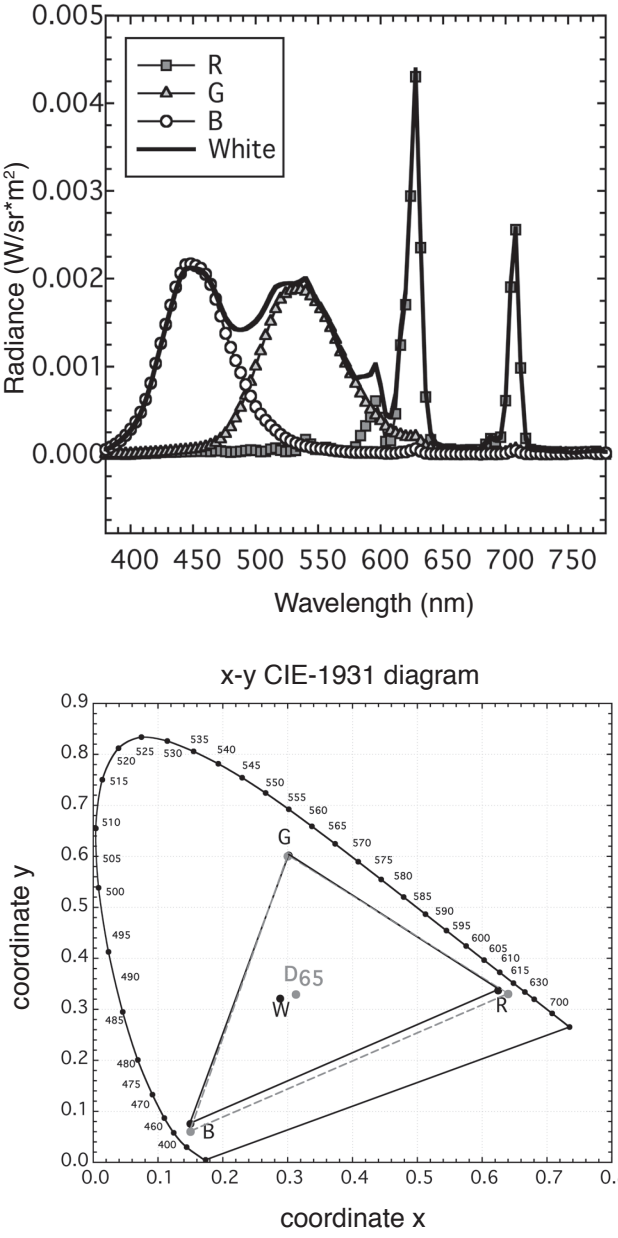

Figure 6. (a) Spectral emission of the primaries and white of the monitor used and (b) chromaticity coordinates of the primaries and white of the monitor used (black circles and solid line), and the standard monitor sRGB (gray circles and dashed line).

Finally, we summarize the overall transformation process of the signals as follows:

sRGB Space

$$k_{NIR} \equiv \left(\frac{L}{L_{\max}}\right)_k = \left(g_k \cdot NDO_{k_{NIR}} + o_k\right)^{\gamma_k}, \tag{7}$$

$$\begin{bmatrix} X_{D65} \\ Y_{D65} \\ Z_{D65} \end{bmatrix} = \begin{bmatrix} 41.23 & 35.76 & 18.05 \\ 21.26 & 71.52 & 7.22 \\ 1.93 & 11.92 & 95.06 \end{bmatrix} \cdot \begin{bmatrix} R_{NIR} \\ G_{NIR} \\ B_{NIR} \end{bmatrix}, \tag{8}$$

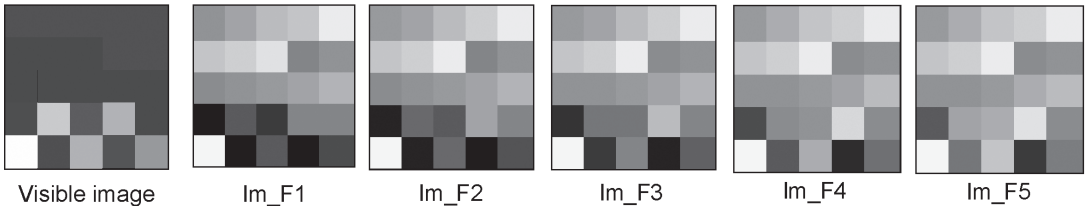

Figure 7. Visible image and five NIR monochromatic images of the twenty-five textile samples. *Supplemental Material—Figure 7 can be found in color on the IS&T website (www.imaging.org) for a period of no less than two years from the date of publication.*

where $k = R$, G and B, $g_k = 0.95$, $o_k = 0.05$ and $\gamma_k = 2.40$ (parameters of calibration of the sRGB standard monitor), and NDO_{kNIR} are the original, normalized, digital output levels, and X_{D65}, Y_{D65}, Z_{D65} are in cd/m^2.

Chromatic Adaptation

$$\begin{bmatrix} X_W \\ Y_W \\ Z_W \end{bmatrix} = 105.4 \cdot \mathbf{M_{adapt}} \cdot \frac{1}{80} \begin{bmatrix} X_{D65} \\ Y_{D65} \\ Z_{D65} \end{bmatrix}, \tag{9}$$

$$\mathbf{M}_{\text{adapt}} = \begin{bmatrix} 0.9423 & -0.0307 & 0.0307 \\ -0.0437 & 1.0287 & 0.0118 \\ 0.0038 & -0.0048 & 1.1185 \end{bmatrix}. \tag{10}$$

where 80 and 105.4 cd/m^2 are the maximum luminance of the standard monitor (sRGB) and the monitor Hansol, respectively. $\mathbf{M_{adapt}}$ was calculated using the Bradford chromatic adaptation transform $\mathbf{M_{BFD}}$, that is:

$$\mathbf{M_{adapt}} = \mathbf{M_{BFD}}^{-1} \cdot \begin{bmatrix} L_W/L_{D65} & 0 & 0 \\ 0 & M_W/M_{D65} & 0 \\ 0 & 0 & S_W/S_{D65} \end{bmatrix} \cdot \mathbf{M_{BFD}}, \tag{11}$$

where

$$\begin{bmatrix} L \\ M \\ S \end{bmatrix} = \mathbf{M_{BFD}} \cdot \begin{bmatrix} X/Y \\ Y/Y \\ Z/Y \end{bmatrix} = \begin{bmatrix} 0.8951 & 0.2664 & -0.1614 \\ -0.7502 & 1.7135 & 0.0367 \\ 0.0389 & -0.0685 & 1.0296 \end{bmatrix} \cdot \begin{bmatrix} X/Y \\ Y/Y \\ Z/Y \end{bmatrix}. \tag{12}$$

Monitor Calibration

$$\begin{bmatrix} R_{Monitor} \\ G_{Monitor} \\ B_{Monitor} \end{bmatrix} = \begin{bmatrix} 0.0377 & -0.0180 & -0.0055 \\ -0.0093 & 0.0172 & 0.0001 \\ 0.0003 & -0.0015 & 0.0084 \end{bmatrix} \cdot \begin{bmatrix} X_W \\ Y_W \\ Z_W \end{bmatrix}. \tag{13}$$

$$NDO_{k\,Monitor} = \left(\frac{k_{Monitor}^{\,1/\gamma_k} - o_k}{g_k} \right) \quad \text{if } k_{Monitor} > 0.0031308,$$
$$NDO_{k\,Monitor} = 12.92 \cdot k_{Monitor} \quad \text{if } k_{Monitor} \le 0.0031308. \tag{14}$$

Results

In order to test the method described above, we first simulated five multispectral images corresponding to a set of twenty-five textile samples with different spectral reflectance in the NIR region (Fig. 7). The images were simulated in order to attain a better control over the process of coloration. A pseudo-white balance process was needed in order to obtain equal responses through all channels for a sample with constant spectral reflectance. After that, the five images were combined using the methods described above in order to obtain the pseudo-colored image. This was transformed according to the display unit. Finally, we compared the different possible color representations and quantified the results in terms of colorimetric discrimination using the following parameters:

Pseudo-Color Difference

$$\Delta\tilde{E} = \left\{ \left[\Delta\left(DO_{R\,Monitor}\right) \right]^2 + \left[\Delta\left(DO_{G\,Monitor}\right) \right]^2 + \left[\Delta\left(DO_{B\,Monitor}\right) \right]^2 \right\}^{1/2}, \tag{15}$$

where $DO_{kMonitor}$ are the transformed digital output levels in color channel k.

This parameter mainly provides information on the lightness difference, as well as the chromatic difference. This parameter is calculated using the digital outputs of the channels of the monitor and it does not therefore have a perfect correlation with the visual perception of the image.

RG–RB–GB Contrast

$$C_{RG} = \left| \frac{DO_{R\,Monitor} - DO_{G\,Monitor}}{DO_{R\,Monitor} + DO_{G\,Monitor}} \right|,$$
$$C_{RB} = \left| \frac{DO_{R\,Monitor} - DO_{B\,Monitor}}{DO_{R\,Monitor} + DO_{B\,Monitor}} \right|,$$
$$C_{GB} = \left| \frac{DO_{G\,Monitor} - DO_{B\,Monitor}}{DO_{G\,Monitor} + DO_{B\,Monitor}} \right|, \tag{16}$$
$$C_{TOT} = C_{RG} + C_{RB} + C_{GB}.$$

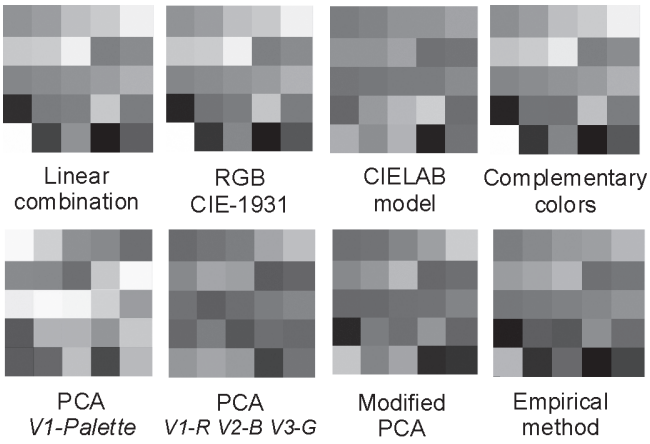

Figure 8. Pseudo-colored images of the twenty-five textile samples obtained applying the various methods. *Supplemental Material—Figure 8 can be found in color on the IS&T website (www.imaging.org) for a period of no less than two years from the date of publication.*

This parameter gives an idea of the nuances or degree of coloration included in the images. The smaller the parameter, the grayer the samples in the pseudo-colored image. This parameter is also calculated using the digital signals of the channels of the monitor.

CIELAB Color Difference

$$\Delta E = \left[(\Delta L^*)^2 + (\Delta C^*)^2 + (\Delta H^*)^2\right]^{1/2} = \left[(\Delta L^*)^2 + (\Delta a^*)^2 + (\Delta b^*)^2\right]^{1/2} \quad (17)$$

As expected, this parameter is most closely correlated to the visual judgments of the resulting pseudo-colored images. In some of the analyses performed, other colorimetric parameters such as luminous contrast (K) (Eq. (18)), lightness difference (ΔL^*), chroma difference (ΔC^*), and hue difference (ΔH^*) were also used.

$$K = \frac{L_{S1} - L_{S2}}{L_{S1} + L_{S2}}. \quad (18)$$

L_{S1}, L_{S2} represent the lightness values of two different samples.

The CIELAB color differences between samples were measured by displaying the images on the monitor and using a telespectracolorimeter (PhotoResearch PR-650). The white of the Hansol monitor was used as the reference white in the corresponding calculations.

The pseudo-colored images obtained for the twenty-five samples with the various methods proposed are shown in Fig. 8. The pseudo-colored images obtained using the first linear combination (Eq. (1)) and the RGB CIE-1931 method are presented. As can be seen, they provide very similar results. In general, very similar pseudo-colored images are achieved by all the linear combinations tested. Examples of color appearance models, specifically *ATD* models, include the Hurvich–Jameson model, Guth et al., Ingling and Tsou. and CIELAB, which were also evaluated. In the figure, the CIELAB model is shown because it provides the best results. The complementary colors model is also presented, as well as methods which use PCA analysis: PCA *V1-Palette*, the specific case of PCA *V1-R*, *V2-B*, *V3-G*, the modified PCA method and, finally, the empirical method with coefficients 0.1 and 0.9.

TABLE III. Parameters of Quantification of the Color Differences: Pseudo-Color Difference, RG-RB-GB Contrast and CIELAB Color Difference (Mean and Standard Deviation of the Twenty-Five Simulated Textile Samples)

METHOD	Pseudo-color difference (ΔE)	RG-RB-GB Contrast (C_{TOT})	CIELAB color difference (ΔE)
Linear Combination	111.38 ± 76.79	0.2499 ± 0.3787	30.76 ± 19.22
RGB CIE-1931	115.55 ± 79.69	0.2516 ± 0.3833	32.36 ± 20.31
CIELAB model	83.06 ± 57.15	0.3360 ± 0.5404	29.99 ± 21.68
Complementary colors	109.40 ± 78.71	0.1309 ± 0.1980	27.75 ± 18.66
PCA *V1-Palette*	213.43 ± 116.97	Ind.*	101.1 ± 59.98
PCA *V1-R V2-B V3-G*	104.94 ± 59.70	0.6526 ± 0.5553	50.83 ± 39.42
Modified PCA	104.33 ± 63.97	0.5110 ± 0.5340	39.97 ± 30.50
Empirical Method (0.1–0.9)	125.60 ± 89.02	0.5275 ± 0.2496	41.55 ± 29.76

*Ind.: Indeterminate. The parameter cannot be calculated because the denominator is 0 in many cases (some colors of the palette used have null digital values for different channels).

TABLE IV. Luminous Contrast (K), Chroma Difference (ΔC^*) and Hue Difference (ΔH^*) (Mean and Standard Deviation of the Twenty-Five Simulated Textile Samples)

METHOD	K	ΔC^*	ΔH^*
Linear Combination	0.22 ± 0.20	14.85 ± 14.07	4.55 ± 4.87
RGB CIE-1931	0.25 ± 0.24	15.05 ± 14.99	4.57 ± 4.99
CIELAB model	0.15 ± 0.17	20.51 ± 20.55	8.85 ± 8.58
Complementary colors	0.24 ± 0.22	8.65 ± 7.18	4.38 ± 5.04
PCA *V1-Palette*	0.23 ± 0.17	20.29 ± 17.10	90.82 ± 59.92
PCA *V1-R V2-B V3-G*	0.14 ± 0.10	20.97 ± 25.12	38.95 ± 34.53
Modified PCA	0.18 ± 0.16	15.97 ± 17.74	25.98 ± 28.50
Empirical Method (0.1–0.9)	0.22 ± 0.19	19.56 ± 13.44	24.93 ± 29.54

The quantification of the colorimetric differences for the examples presented, that is, the pseudo-color difference, RG-RB-GB contrast and CIELAB color difference, are summarized in Table III. Table IV shows the detailed results of the luminous contrast, hue and chroma differences. The best results in terms of visual discrimination are achieved by methods based on PCA. With these methods, the CIELAB color differences have maximum values, basically using the method which associates the first principal vector with a color palette (PCA *V1-Palette*). The greater contribution towards this color difference is due to the considerable differences in hue between samples that this class of methods achieves. In general, with these methods, the RG-RB-GB contrasts also have large values. This means that the pseudo-colored samples belonging to the images do not have neutral colors. For the *PCA V1-Palette* method, the RG-RB-GB contrast cannot be calculated: the denominator is 0 in many cases because some of the colors of the palette used have null digital values for different channels. The largest pseudo-color difference is also achieved with the PCA *V1-Palette* method. The results obtained with the PCA *V1-R V2-B V3-G* method are not as good as when using PCA *V1-Palette*. However, this method is preferable if the aim is to discriminate between samples with very similar reflectance spectra, because more information is used (principal vectors *V2*

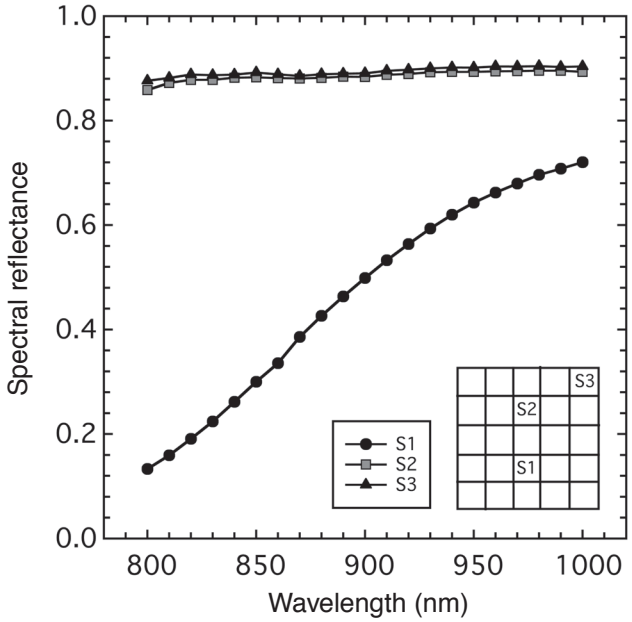

Figure 9. Spectral reflectance curves for samples S1, S2 and S3.

TABLE V. Lightness, Chroma and Hue Angle Values for Samples S1, S2, and S3.

METHOD	SAMPLE	L^*	C^*	h (°)
Linear Combination	S1	50.48	49.70	81.85
	S2	87.88	1.86	105.15
	S3	88.12	0.96	104.32
PCA *V1-Palette*	S1	90.29	72.58	151.78
	S2	35.41	70.41	52.83
	S3	34.87	65.71	34.18
PCA *V1-R V2-B V3-G*	S1	38.42	110.20	309.00
	S2	63.70	25.81	65.10
	S3	74.09	38.76	106.93

TABLE VI. CIELAB Color Differences ΔE (Mean and Standard Deviation) of the Four Real Textile Samples (Examples 1 and 2) and the Four Marked Zones of the Landscape Image

METHOD	Example 1	Example 2	Landscape
Linear Combination	11.65 ± 7.28	30.59 ± 14.78	19.27 ± 9.01
Complementary colors	12.61 ± 8.16	27.01 ± 14.60	16.65 ± 97
PCA *V1-Palette*	54.24 ± 34.81	69.98 ± 39.30	82.38 ± 49.12
PCA *V1-R V2-G V3-B* (Example 1 and Landscape) *V1-G V2-R V3-B* (Example 2)	22.26 ± 16.56	39.581 ± 22.83	33.09 ± 15.02

and *V3*). The colorimetric parameters obtained using the modified PCA method are not as good as for the rest of the methods mentioned above. However, the samples with fairly constant spectral reflectance preserve similar tones, meaning that some spectral information is kept. With the empirical method, the results obtained do not justify the long computation time needed.

The methods which attempt to imitate human color vision do not have large CIELAB color differences and RG-RB-GB contrasts, but they do carry spectral information on the pseudo-colored samples. The corresponding hue differences are small, the contribution to color differences due to luminous contrast and chroma differences being greater. However, the chroma differences achieved are generally smaller than those obtained using PCA-based methods. As shown in Fig. 8, these methods provide images with many samples colored with neutral tones. This can be explained by the flat profile of the reflectance spectra of these samples in the NIR region (garnet and blue samples in the visible image). Although the spectra of these samples is almost constant, they present different reflectance values in the NIR region. Therefore, they result in a different gray level and can be differentiated, while they are indistinguishable in the visible region. The other samples of the image, which generally appear reddish, have greater spectral reflectances at longer wavelengths. Some of these methods, such as linear combination and RGB CIE-1931, have large values for the pseudo-color difference parameter. As previously stated, this parameter essentially accounts for the lightness changes, as well as the chromatic differences.

Figure 9 shows the spectral reflectance curves for three samples. In Table V, the lightness, chroma and hue values for each sample are shown. Using linear combination, the chroma values for samples S2 and S3 are small due to the neutral coloration, because of their flat spectral profile. Sample S1, however, has a larger chroma value, showing the higher spectral purity of its reflectance. With the PCA *V1-Palette* method, larger values of chroma result for the three samples, thus disregarding the associated spectral information. Samples S2 and S3 have similar pseudo-colors with the linear method, because of the similarity of their reflectance spectra (ΔE = 0.92). Using the PCA *V1-R V2-B V3-G* method, a considerable CIELAB color difference is achieved (ΔE = 28.04), while the PCA *V1-Palette* method yields a smaller difference, since only the first principal component is used (ΔE = 5.91). The PCA *V1-R V2-B V3-G* method yields very different hue angles between these two samples, due to the use of the second and third principal components, so the color differences increase.

Once the simulations were performed, we used the multispectral system[4–6] developed to experimentally capture various images corresponding to real samples, and applied the methodologies that were shown to achieve the best results. First of all, we analyzed some of the real textile samples which had been simulated beforehand, some of them with a fairly constant spectral reflectance (Example 1) and others with increasing spectral reflectance (Example 2). The results obtained can be seen in Fig. 10. We also analyzed an image of a landscape (Fig. 11) in order to show the utility of the methods for any type of image. The CIELAB color differences obtained between samples in all the experimental images are shown in Table VI. For the images of textile samples, each of the four samples were tested. For the landscape image, the zones analyzed are marked on the corresponding figure. Experimentally, the texture, inhomogeneities etc. can affect the coloration of the object. For this reason, some of the samples do not appear pseudo-colored in a uniform way. As in the simulations, the best color representations in terms of visual discrimination, that is, maximum CIELAB color differences between samples, were achieved by methods based on PCA analysis, mainly with the PCA *V1-Palette* method. The methods related to human color vision provide spectral information of the samples in the NIR region. Thus, the samples belonging to Examples 1 and 2 appear grayish and reddish, respectively,

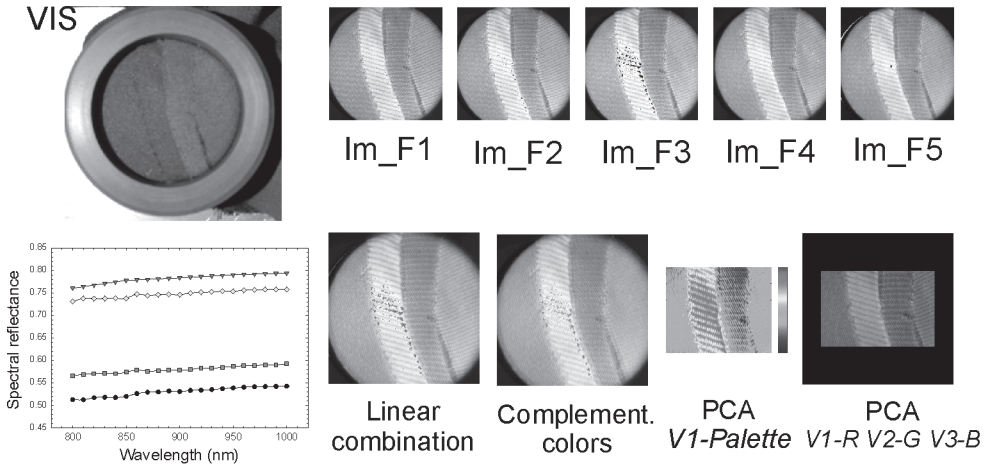

(a)

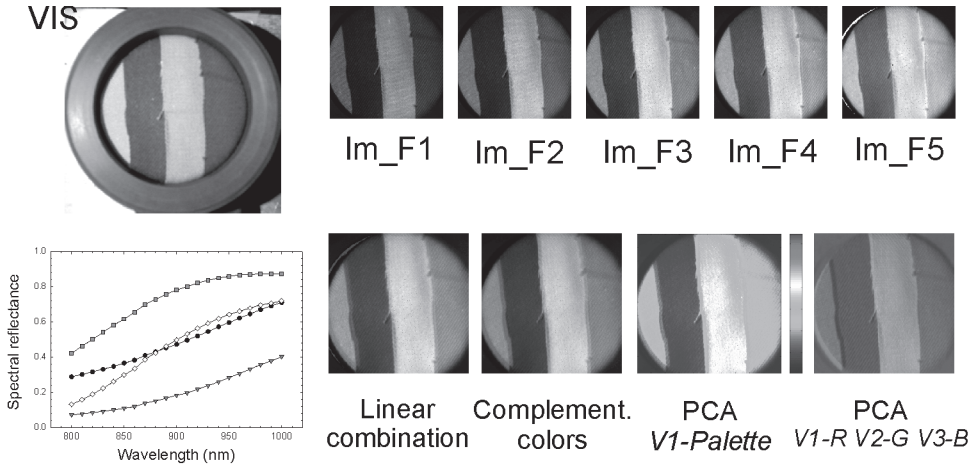

(b)

Figure 10. Visible image, spectral reflectance curves, NIR multispectral images, and pseudo-colored images obtained using various methods of four real textile samples (a) samples with a fairly constant spectral reflectance (Example 1) and (b) samples with an increasing spectral reflectance (Example 2). *Supplemental Material—Figure 10 can be found in color on the IS&T website (www.imaging.org) for a period of no less than two years from the date of publication.*

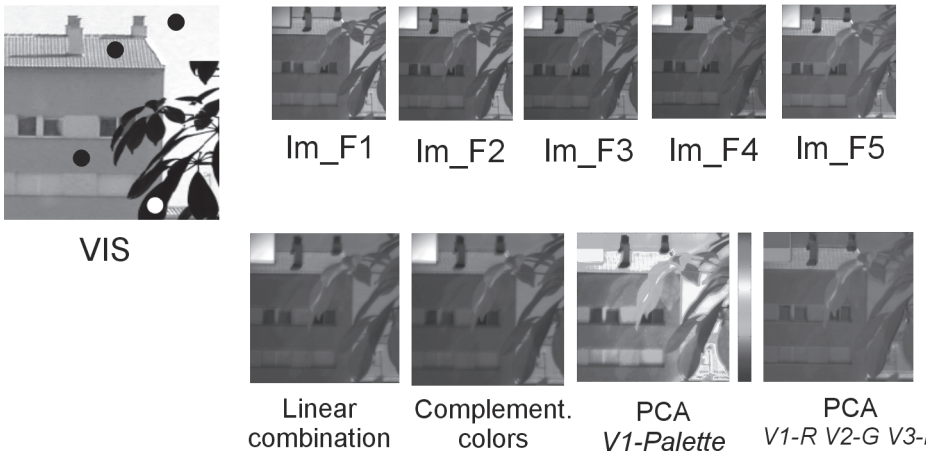

Figure 11. Visible image, NIR multispectral images, and pseudo-colored images of a landscape. *Supplemental Material—Figure 11 can be found in color on the IS&T website (www.imaging.org) for a period of no less than two years from the date of publication.*

according to their spectral reflectance curves also shown in the figures. On the other hand, it can be seen that, in the landscape images, and using methods related to human color vision, the sky appears bluish. This can be explained by its spectral emission, which is decreasing in the visible region but also preserves this tendency along the NIR range.

To summarize, depending on whether we want to imitate human color vision or to discriminate between samples, two different methods are possible. Because of the correlation of the spectral bands in the NIR region of many samples, due to the constant nature of their spectral reflectance profiles, many pseudo-colored objects obtained using the first type of methods are neutral. If decorrelation methods are used instead, it is easier to discriminate between the samples. However, with the first kind of method, spectral information of reflectance of the samples is provided.

Conclusions

We have developed a color visualization system for multispectral images in the NIR region of the electromagnetic spectrum (800–1000 nm). The pseudo-coloration process of the images was divided into two stages: 1) definition of the color representation space, for which different combinations of the NIR images were proposed in order to obtain the signals R_{NIR}, G_{NIR} and B_{NIR}, that allow us to obtain a pseudo-colored image; and 2) calibration of the visualization device, in which the last signals were conveniently transformed in order to obtain similar chromatic sensations with any visualization device. For the first stage, several pseudo-coloring methods were proposed; some of these attempt to imitate human color vision and others were based on decorrelation methods (PCA). For the second stage, a GOG (gamma, offset, gain) model was used to calibrate a CRT monitor in which the color images were displayed. Finally, we performed simulations and experimental acquisitions, making use of a multispectral system that we developed, of several samples with different reflectance spectra in order to analyze the methodologies proposed. The pseudo-colored images were analyzed numerically, using several parameters such us contrast levels and color differences. As expected, the parameters that achieved the best results in terms of correlation with the visual judgments were the CIELAB color differences. The methods based on PCA analysis provided the best results regarding discrimination between the samples (with the greatest CIELAB color differences). On the other hand, the methods related to human color vision carry information on the spectral reflectances of the samples, and this can be useful for specific applications. The techniques presented would allow users to distinguish between samples with the same appearance in the visible region but different spectral reflectance in the NIR region.

Acknowledgment. This research was funded by the Spanish Ministry for Science and Technology (Ministerio de Ciencia y Tecnología) under grant number DPI2002-00118. M. Vilaseca would like to thank the Generalitat (government) of Catalonia for the Ph.D. grant that she received.

References

1. J. M. Pope, NIR gains continue in on-line process applications, *Chiltons I&CS* **67,** 45 (1994).
2. M. Matsuoka, *Infrared Absorbing Dyes*, Plenum Press, New York, 1990.
3. D. A. Burns and E. W. Ciurczak, *Handbook of Near-Infrared Analysis*, NIR Publications, Chichester, West Sussex, 1999.
4. M. Vilaseca, J. Pujol and M. Arjona, Illuminant influence on the reconstruction of near-infrared spectra, *J. Imaging Sci. Technol.* **48,** 111 (2004).
5. M. Vilaseca, J. Pujol and M. Arjona, Spectral-reflectance reconstruction in the near-infrared region by use of conventional charge-coupled- device camera measurements, *Appl. Opt.* **42,** 1788 (2003).
6. M. Arjona, M. Vilaseca, and J. Pujol, Multispectral system for recovering near-infrared reflectance spectra, in *Proc. of the Second European Conference on Colour in Graphics, Imaging and Vision*, IS&T, Springfield, VA, 2004, pp. 409–413.
7. D. Scribner, P. Warren, J. Schuler, M. Satyshur, and M. Kruer, Infrared color vision: an approach to sensor fusion, *Optics & Photonics News* **9,** 27 (1998).
8. D. Scribner, P. Warren and J. Schuler, Extending color vision methods to bands beyond the visible, *Machine Vision Appl.* **11,** 306 (2000).
9. J. M. Artigas, P. Capilla, A. Felipe, and J. Pujol, *Óptica Fisiológica: Psicofísica de la visión*, McGraw-Hill Interamericana de España, Madrid, 1995.
10. M. D. Fairchild, *Color Appearance Models*, Addison-Wesley, Reading, MA, 1998.
11. R. C. Gonzalez and R. E. Woods, Digital image processing, Addison-Wesley, Reading, MA, 1993.
12. I. T. Jolliffe, *Principal Component Analysis*, Springer-Verlag, New York, NY, 1986.
13. CIE 122-1996, The relationship between digital and colorimetric data for computer-controlled CRT displays.
14. R. S. Berns, Methods for characterizing CRT displays, *Displays* **16,** 173 (1995).
15. D. H. Brainard, D. G. Pelli and T. Robson, *Display characterization. Encyclopedia of Imaging Science and Technology*, Wiley, New York, NY, 2002, p. 172.
16. G. Wyszecki, *Color Science: Concepts and Methods, Quantitative Data and Formulae*, John Wiley and Sons, New York, NY, 1982.
17. J. M. Artigas, P. Capilla and J. Pujol, *Tecnología del Color*, Publicacions de la Universitad de Valéncia, Valéncia, España, 2002.
18. Photographic and Imaging Manufacturers Association, Inc., PIMA 7667:2001, Photography -Electronic still picture imaging - Extended sRGB color encoding - e-sRGB. PDF file, available online at http://www.srgb.com/whatsnew.html [consulted 16 June 2004].
19. M. Stokes, M. Anderson, S. Chandrasekar, and R. Motta, *A standard default color space for the Internet – sRGB*, International Color Consortium Report, 1996. URL http://www.color.org/sRGB.html [consulted 16 June 2004]..
20. R. S. Berns, *Principles of Color Technology*, John Wiley and Sons, New York, NY, 2000.
21. C. Li, M. R. Luo, B. Rigg, and R. W. G. Hunt, CMC 2000 chromatic adaptation transform: CMCCAT2000, *Color Res. Appl.* **27,** 49 (2002).
22. N. Moroney, M. D. Fairchild, R. W. G. Hunt, C. Li, M. R. Luo, and T. Newman, The CIECAM02 color appearance model, in *Proc. of the IS&T/SID Tenth Color Imaging Conference*, IS&T, Springfield, VA, 2004, pp. 23–27.